crystals

MDPI

Article

Research on the Impact-Induced Deflagration Behavior by Aluminum/Teflon Projectile

Jianguang Xiao [1,2,*], Yanxin Wang [1], Dongmo Zhou [1], Chenglong He [1,2] and Xiangrong Li [3,*]

[1] College of Mechatronic Engineering, North University of China, Taiyuan 030051, China; s2001135@st.nuc.edu.cn (Y.W.); zhoudongmo@nuc.edu.cn (D.Z.); hechenglong@bit.edu.cn (C.H.)
[2] Science and Technology on Transient Impact Laboratory, No. 208 Research Institute of China Ordnance Industries, Beijing 102202, China
[3] Department of Weapons and Control, Academy of Armored Force Engineering, Beijing 100072, China
* Correspondence: xiaojg@nuc.edu.cn (J.X.); lixiangrong2022@gmail.com (X.L.)

Abstract: Although the ignition-and-growth model can simulate the ignition and detonation behavior of traditional energy materials well, it seems insufficient to simulate the impact-induced deflagration behavior of reactive materials (RMs) using current finite element codes due to their more complicated ignition threshold and lower reaction rates. Therefore, a simulation method for the impact-induced deflagration behavior of a reactive materials projectile (RMP) is developed by introducing tunable ignition threshold conditions for RMs, and a user-defined subroutine is formed by the secondary development on the equation of state (EOS). High-velocity impact experiments were performed to prove the validity of simulations. The results show that the user-defined subroutine for RMs is competent in simulating the ignition and deflagration behavior under impact conditions, because the reaction ratio, morphology and temperature distribution of RMP fragments are all well consistent with experiments, theory, and current reports from other researchers. In this way, the quantitative study on the deflagration reaction of RMs can be implemented and relevant mechanisms are revealed more clearly.

Keywords: reactive materials; impact-induced deflagration; simulation; ignition behavior; reaction ratio; temperature distribution

Citation: Xiao, J.; Wang, Y.; Zhou, D.; He, C.; Li, X. Research on the Impact-Induced Deflagration Behavior by Aluminum/Teflon Projectile. *Crystals* **2022**, *12*, 471. https://doi.org/10.3390/cryst12040471

Academic Editors: James L. Smialek, Yong He, Wenhui Tang, Shuhai Zhang, Yuanfeng Zheng and Chuanting Wang

Received: 9 February 2022
Accepted: 26 March 2022
Published: 28 March 2022

1. Introduction

When perforating or penetrating the intended target, reactive materials (RMs) will chemically react due to the shock wave passing through them, thereby increasing the damaging effects from the combination of the kinetic energy (KE) and chemical energy (CE) of a reactive projectile [1–3]. RMs are a class of shock-induced energetic materials, including thermites, intermetallics, metal-polymer mixtures, metastable intermolecular composites (MICs), and so on. With the benefit of fine mechanical and chemical performance, polytetrafluoroethylene based RMs have been extensively researched recently. In order to investigate their lethality, ground tests have been conducted, and several physics-based models were established [4–8]. However, RMs are generally formulated to release appreciable CE under intense dynamic loads (such as high-velocity impact or detonation), so the activation time is extremely short, making the measurement of many physical quantities very difficult. Consequently, an appropriate analytical tool for RMs is required to predict target damage beyond that measured under experimental conditions [3]. Popular dynamic calculation codes, such as ANSYS-Autodyn or Ls-dyna, were employed to predict the response of energetic materials. In these codes, the simulation results are dependent on an appropriate material model, which includes the equation of state (EOS), strength model, failure model, erosion model, and so on. Researchers have paid close attention to the material model of RMs.

For the unreacted reactant of RMs, the shock EOS model was used to research the critical velocity of the reactive materials projectile (RMP) to initiate the covered explosive [9,10], and Instron compression tests and high-rate split Hopkinson bar experiments were carried out to determine the parameters of the Johnson–Cook strength model, which can be used to effectively simulate the deformation and penetration behavior of reactive materials [11,12]. For reaction product, the Jones–Wilkins–Lee (JWL) EOS was used to characterize the expansion behavior after the chemical reaction of RMs [13]. In fact, compared to the KE damage caused by traditional inert metal materials, it is mainly the CE that causes the remarkably high-efficiency damage during the impact events of RMs. The ignition time, reaction rate, reaction efficiency, and so on, play an important part in the energy release of CE. In particular, the initiation criterion, which is characterized by the values of the impact pressure P and its duration τ or by the values of an impacting projectile's velocity V and diameter d ($P^2\tau$ or V^2d criteria), significantly influences the damage event of RMs. The forest fire model was provided and developed to match pressure–time data obtained from gauges embedded in the energetic materials in a broader set of experiments [14]. Recently, the Naval Surface Warfare Center has estimated the impact velocity and pressure initiation threshold of reactive materials with different particle size with a gas gun experiment [15,16]. They found that the initiation reaction occurs earlier in reactive materials with smaller particle size; this is mainly induced by the shear band formed in the impact event, and empirical formulas ($t^a(\sigma-\sigma_{TS})^b = c$)) were proposed to characterize the ignition behavior of Al/PTFE reactive materials.

The above literature reviews show that the EOS and ignition model for RMs have been improved. However, an integrated, analytical method to reproduce the high-efficiency damage caused by RMs has not been presented, to the best of our knowledge. In past decades, relevant simulations often divided the damage event into two relatively independent phases. For example, the damaging effects on concrete targets produced by reactive material liner shaped charges were researched by dividing the physical process into an inert impact-penetration stage and an internal deflagration stage for RMs. The shock model was used to simulate the inert penetration behavior of RMs, and either the JWL or powder burn model was used to simulate the internal deflagration behavior of RMs [17–20]. Although the Lee–Tarver model embedded in Autodyn or Ls-dyna can characterize the detonation performance of high explosives, no interface is provided to adjust the initiation criterion that is crucial to simulate the damage event for RMs.

The purpose of this effort is to combine the divided stages into one by developing the EOS subroutine based on Autodyn code; then, quantitative research of real-time reaction can be conducted by using the tunable ignition criteria. A simulation method is proposed to investigate the impact-induced deflagration behavior of polytetrafluoroethylene based RMP. This work is of great value in the design of RMPs and understanding their damage mechanisms more clearly.

2. Experiment

2.1. Specimen Preparation

The Al/PTFE RMPs were prepared by the process of mechanical mixing–cold pressing–sintering. First, the raw Al and PTFE powders, with Al particle size of 5 μm and PTFE particle size of 34 μm (the purity of Al and PTFE are above 98% and 99%, respectively, according to the vendor's description), were poured into a container where they were mechanically stirred with a rotation speed of approximately 20,000 rpm. Then, the symmetrical distribution powders were poured into a cold-pressing mold where the pressure was loaded by a puncher pin on the powders with a linear speed of 5 mm/min. When the pressure reached approximately 1 MPa, the load speed of the puncher pin was controlled by pressure increments at approximately 1 MPa/s. The puncher pin did not stop until the pressure reached 100 Mpa; subsequently, the pressure was kept at this level for 1 min. In this way, the powders were pressed into a cylinder, then inserted into a vacuum sintering oven. The oven temperature rose to 375 °C at a rate of 60 °C/h and stayed at 375 °C for

0.5 h. After that, the oven temperature dropped to 327 °C at a rate of 40 °C/h and stayed at 327 °C for 1 h. Lastly, during the cooling process, the oven temperature dropped to ambient temperature at an average rate of approximately 50 °C/h. The density of the RMP fabricated by this method is close to the theoretical maximum density of 2.27 g/cm^3.

2.2. Experiment Setup

The experiment system was mainly composed of the one-stage gas gun, laser speed detector, chamber, double-spaced Al plates holder, and high-speed camera, as shown in Figure 1. After the projectiles were launched by the one-stage gas gun, the two laser beams (laser speed detector) recorded the speed of the projectiles. An on–off signal, produced by the veil effect of the projectiles on the laser beams, was used to trigger a high-speed camera; consequently, the images of the penetration and deflagration behavior of the RMPs on the double-spaced Al plates was recorded. Eight shots, with the impact velocity ranging from 293 to 652 m/s, were performed to investigate the penetration and deflagration behavior of RMs. Several square Al plates with a size of 400 × 400 mm^2 were used in this study and the distance between the front and rear plate was 200 mm. The size of the projectiles is listed in Figure 1. The penetration hole and bulges on the front plate (FP) and rear plate (RP) were used to characterize the penetration behaviors of RMPs and damage effects of the double-spaced Al plates, while the duration and size of the flame, resolved by high-speed camera, were used to characterize the deflagration behavior of RMPs.

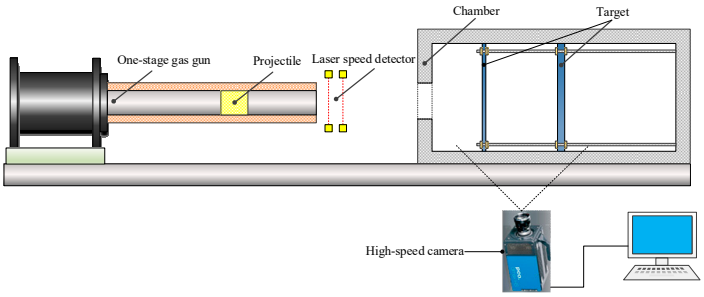

Figure 1. Schematic diagram of experimental setup.

2.3. The Damage Effects of Double-Spaced Al Plates

In the eight experiments with velocities ranging from 293 to 652 m/s, all front plates were perforated, while petalling or plugging damage formed on the backside of the front plates, depending on the various impact velocities. It is worth noting that there was a plastic zone (between the red and yellow dotted line in Figure 2) in the vicinity of the penetration hole in both petalling and plugging damage. On the rear plates, considerable soot was produced on the frontside because of the chemical reaction by residual RMPs, while various degrees of bulges were formed on the backside. The typical damage patterns and details on damage effects are shown in Figure 2 and Table 1, respectively.

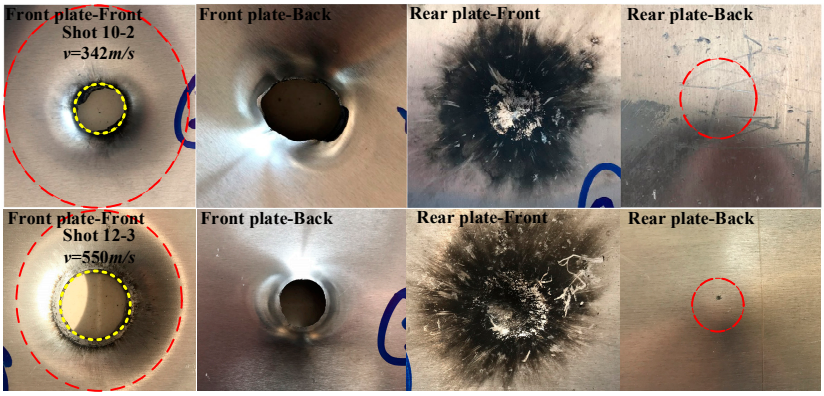

Figure 2. The damage patterns on the front and rear plate in shots 10-2 and 12-3.

Table 1. Experimental results.

Shot	Projectile Size ($\Phi D \times L$) (mm)	Velocity (m/s)	Penetration Hole Diameter on FP (mm)	Deflagration Time (μs)		
				Perforating FP	Impacting on RP	Fades Away
10-1	15.40 × 15.39	293	~15.47	210.24	210.24	1629.35
10-2	15.39 × 15.38	342	~18.01	420.48	998.63	5045.73
10-3	15.40 × 15.36	401	~24.53	367.92	2890.78	8672.34
10-4	15.41 × 15.21	397	~20.06	473.04	3521.50	9040.26
12-1	15.40 × 7.64	652	18.62	252.39	378.58	8539.10
12-2	15.50 × 7.76	570	18.73	294.45	3070.71	7697.81
12-3	15.50 × 7.80	550	17.33	210.32	252.39	4374.71
12-4	15.40 × 7.30	620	19.37	126.19	1724.65	8286.71

Notes: FP and RP represent the front and rear plate, respectively. The deflagration time means the duration of deflagration of RMs: (1) perforating FP means the whole deflagration time caused by the penetration to FP; (2) impacting RP means the time required for the reaction to increase to maximum from the impact on RP; and (3) fade away means the time from peak to end of deflagration reaction.

3. Numerical Simulation

3.1. Reaction Model of Energy Release Process by RMs

The impact-induced energy release process of RMs can be summarized as follows: (1) the fragmentation of RM samples; (2) the product of small gas molecules from the decomposition of the fluoropolymer matrix under impact loading (impact-induced hotspot or impact-induced fracture); (3) the exposure of reactive metal to small gas molecule atmospheres; and (4) the burning process of the fragmentized composite particle. For numerical simulations at the macro scale, the decomposition of the fluoropolymer matrix and the exposure of reactive metal to small gas molecule atmospheres are usually simplified, and attributed either to stress concentrated in a local point or temperature. When the stress or temperature achieve a threshold value, it is considered evidence that the decomposition of fluoropolymer matrix and exposure of reactive metal to small gas molecule atmospheres have occurred. In this way, the phenomenological research can be conducted based on any ignition criterion. However, no apparent interfaces are provided to adjust the ignition criterion in the ignition-and-growth model in Ls-dyna or Autodyn, which are commonly used to conduct simulations of the impact-induced burning process of energetic materials. Consequently, some modifications are required to simulate the impact-induced deflagration reaction of RMs.

In Autodyn code, the EOS subroutine is used to calculate pressure, energy, and sound speed as a function of density. When the density of the current timestep is updated and retrieved from the main program, the new pressure, energy, and sound speed can be updated by the EOS model, then returned to the main program to calculate other variables. In the energy release process of RMs, they undergo three material states, including solid reactant state, solid-gas mixing state, and gas state, in the same particle. Therefore, three different EOSs are generally needed to model the distinct states, which makes the solving process complex and expensive. To solve this issue, reaction ratio F is introduced to couple the equations of state (EOSs) for reactant and reaction product, based on the assumption of pressure and heat balance. After iterative computations on pressure and temperature, the reaction ratio, energy, and sound speed can be updated; this is discussed in detail in Section 3.1.5. In this way, a unitary EOS or reaction model was proposed to describe the mixture in the reaction zone [21].

3.1.1. EOS of Unreacted Reactant

For unreacted reactant, a shock EOS is employed to describe the pressure state under impact condition, which takes the following form [9]

$$P_u(V_u, T) = P_H(V_u) + \frac{\rho_0 \Gamma}{V_u}(E - E_H) = P_H(V_u)\left(1 - \frac{\Gamma}{2}\frac{1 - V_u}{V_u}\right) + \frac{\rho_0 \Gamma}{V_u} C_{v,u} T \quad (1)$$

where $\begin{cases} P_H(V_u) = \rho_0 c_0^2 (1 - V_u)/[1 - s(1 - V_u)]^2 & V_u \le 1 \\ P_H(V_u) = \rho_0 c_0^2 (\eta_u - 1) & V_u > 1 \end{cases}$.

where subscript u denotes unreacted reactant, Γ is the Grüneisen coefficient, T is temperature, ρ_0 and c_0 are the initial density and elastic wave velocity of the reactant, respectively, $C_{v,u}$ is the specific heat capacity, and s is the slope of the shock velocity or particle velocity fit. E_H is the specific internal energy, which can be calculated as

$$\begin{cases} E_H(V_u) = \frac{1}{2}\{c_0(1 - V_u)/[1 - s(1 - V_u)]\}^2 & V_u \le 1 \\ E_H(V_u) = \frac{1}{2} c_0^2 V_u \left(\frac{1}{V_u} - 1\right)^2 & V_u > 1 \end{cases} \quad (2)$$

3.1.2. Ignition Criterion

The chemical reaction of RMs occurs when the particles obtain enough energy. Generally, mechanical, thermal, optical, electrical, chemical, and acoustic stimuli can cause the ignition of RMs. Under the impact-initiation scenario, ignition behavior often occurs in the shear band, so the peak stress has been employed to judge the appearance of the ignition event by the Naval Surface Warfare Center [15,16]. They point out that the RMs do not ignite at the beginning of the collision, but have an ignition delay time, which can also be interpreted as the time for the material to absorb energy under certain stress conditions. As described in Equation (3), when the stress exceeds the ignition threshold σ_{TS}, the term that represents the impulse on the left side of the equation accumulates with time. When it reaches a constant c, the local RMs may be ignited. In contrast, the ignition of RMs substantially starts with the decomposition reaction of fluorine polymer. When the instantaneous temperature reaches the critical decomposition temperature, the chemical reaction may also be stimulated. Therefore, the following expression is used to model the ignition behavior for RMs.

$$t^a(\sigma - \sigma_{TS})^b = c \quad or \quad T = T_d \quad (3)$$

where σ and σ_{TS} are real-time stress and ignition threshold stress, respectively; t is accumulated time in which the σ exceeds σ_{TS}; a, b, and c are constants; T is instantaneous temperature; and T_d is critical decomposition temperature of fluorine polymer contained in RMs.

3.1.3. EOS of Reaction Product

The JWL EOS is usually used to describe the state of the reaction product. The pressure and specific internal energy, respectively, can be calculated as follows [22]

$$P_p(V_p, T) = Ae^{-R_1 V_p} + Be^{-R_2 V_p} + \frac{\omega \rho_0}{V_p} C_{v,p} T \quad (4)$$

$$E_p(V_p, T) = \left(\frac{A}{R_1} e^{-R_1 V_p} + \frac{B}{R_2} e^{-R_2 V_p}\right)/\rho_0 + C_{v,p} T \quad (5)$$

where subscript p denotes reaction product and A, B, R_1, R_2, and ω are constants.

3.1.4. Reaction Rate

The ignition-and-growth model of explosive initiation is employed to characterize the impact-induced initiation behavior of RMs. The chemical reaction rate for the conversion from unreacted explosive to reaction product consists of three physically realistic terms: an ignition term of a small explosion occurs soon after the shock wave; a slow growth term of

reaction speed as this initial reaction goes on; and a reaction completion term with a rapid reaction rate. The form of the reaction rate equation is [9]

$$\frac{dF}{dt} = I(1-F)^b\left(\frac{\rho}{\rho_0} - 1 - a\right)^x + G_1(1-F)^c F^d P^y + G_2(1-F)^e F^g P^z \quad (6)$$

where I, G_1, G_2, a, b, c, d, e, g, x, y and z are adjustable coefficients for energetic materials. $F = 0$ indicates the reactant did not react, and the variables are calculated by the equations of unreacted reactant. $F = 1$ indicates the chemical reaction is complete, and the variables are calculated by the equations of reaction product. If $0 < F < 1$, this indicates the chemical reaction is ongoing and the mixture is made of reactant and deflagration product, and the variables are calculated by introducing a mixing rule.

The three portions of the ignition-and-growth model exhibit distinguished chemical reaction rates during the three physically realistic terms discussed above. This model contains three more parameters: FMXIG, FMXGR, and FMNGR. The ignition rate is set equal to zero when $F \geq$ FMXIG, the growth rate is set equal to zero when $F \geq$ FMXGR, and the completion rate is set equal to zero when $F \leq$ FMNGR. Therefore, if no ignition criterion is employed, it is the constant "a" that dominates early ignition reactions, which could be considered the ignition criterion or threshold. When the compression of some particles increases to a value that is large than "a", the chemical reaction rate increases according to the ignition term. At this stage, the slow growth and completion term is approximate to zero as the "F", which is nearly zero in the early phase of ignition. The parameters contained in this model can be obtained through an explosive shock experiment with an iterative approach that adjusts the parameters until the simulation results agree with the test results [14].

3.1.5. Mixing Rule

An EOS subroutine in Autodyn is mainly required to update the specific internal energy and pressure. When $F = 0$ or $F = 1$, relevant calculations can be done by Equations (1), (2), (4) and (5). When $0 < F < 1$, the mixture is composed of unreacted reactant and reaction product. After the reactant is activated, the specific internal energy is defined as

$$E(V, T, F) = (1-F)E_u + FE_p + (1-F)Q \quad (7)$$

where Q is reaction heat released by reactive materials per unit of mass.

During an update process in a calculation circulation of an EOS subroutine, pressure and temperature equilibrium is assumed in the mixture. The temperature is first calculated based on the first law of thermodynamics. The differential form of specific internal energy is

$$\begin{aligned} dE &= \left(\tfrac{\partial E}{\partial V}\right)_{T,F} dV + \left(\tfrac{\partial E}{\partial T}\right)_{V,F} dT + \left(\tfrac{\partial E}{\partial F}\right)_{V,T} dF \\ &= JdV + C_v dT + HdF \end{aligned} \quad (8)$$

According to the first law of thermodynamics, the internal energy absorbed by a small region of the material during a change from one state (or time) to another equals the heat (or energy) input into the region minus the work done by the region in the action of the internal pressure forces. This can be expressed in the relation $dE = -PdV$. Combining this with Equation (8), one can obtain the temperature increment

$$C_v dT = -(P + J)dv - HdF \quad (9)$$

In this paper, the heating effects produced by artificial viscosity and plastic work are included in the simulation, so Equation (9) becomes

$$C_v dT = -(P + J + q)dv - HdF + W_{plstic} \quad (10)$$

where q is artificial viscosity, C_v is constant-volume specific heat of energetic materials.

In this way, the temperature in a small region could be estimated based on the parameters of the former timestep. Then, the pressure of unreacted reactant and reaction product could be obtained by the (V, T) form of EOS, including Equations (1) and (4). The pressures in the unreacted and the gaseous phases of the RMs depend on the relative volume of the two phases, which is defined as follows

$$V = (1 - F)V_u + FV_p \tag{11}$$

When the relative volume of the mixture is returned by main routine, the model iterates on the relative volume of the unreacted reactant until it meets pressure equilibrium with the reaction product, then the derived pressure P is returned. Meanwhile, the specific energies of unreacted and gaseous phases are obtained from Equations (2) and (5). The reaction rate can be calculated by Equation (6), and the specific energy of the mixture is calculated by Equation (7).

Finally, the local sound speed can be estimated as

$$\begin{aligned} c &= \sqrt{\frac{dp}{d\rho}} = \sqrt{\frac{dp}{d\eta} \cdot \frac{d\eta}{d\rho}} = \sqrt{\frac{1}{\rho_0} \cdot \frac{dp}{d\eta}} \\ &= \sqrt{\frac{1}{\rho_0} \cdot \left[(1-F)\left(\frac{\partial p_u}{\partial \eta_u} + \frac{\partial p_u}{\partial T}\frac{\partial T}{\partial E_u}\frac{\partial E_u}{\partial \eta_u}\right)\frac{d\eta_u}{d\eta} + F\left(\frac{\partial p_p}{\partial \eta_p} + \frac{\partial p_p}{\partial T}\frac{\partial T}{\partial E_p}\frac{\partial E_p}{\partial \eta_p}\right)\frac{d\eta_p}{d\eta}\right]} \end{aligned} \tag{12}$$

where $\eta = 1/V$ and subscripts u and p denote the unreacted reactant and reaction product, respectively.

3.1.6. Program Implementation in Autodyn User's Subroutines

Autodyn provides several subroutine interfaces for options such as material models, boundary conditions, and so on. The material model subroutines, such as EOSs, strength models, failure models, and erosion models, are commonly developed depending on user demand. In order to characterize the impact-induced initiation and energy release behavior of RMs, the EOS subroutine, including parameters initialization, parameters check, interfacial design, and solve loop, that dominates the pressure response and energy transformation, is developed in this work. The solve loop of the developed EOS subroutine is listed in Figure 3.

When called by the main program, the EOS subroutine checks whether the current cycle is the first cycle. If so, it initializes user-defined variables to zero, else it retrieves variable values from the previous timestep. Then, it estimates the temperature using Equation (10) so the pressure can be calculated with corresponding EOS models. Meanwhile, the local sound speed of a small region is estimated using Equation (12). Afterward, it updates ignition expression on the left side of Equation (3) using the pressure calculated in the current timestep. If this meets the ignition criterion, it updates the reaction fraction in Equation (6), else it implies the chemical reaction does not occur in this small region. Finally, it updates the specific energy using the new reaction ratio.

3.2. Constitutive Model

During the penetration process, the deformation and yield of materials on the impact interface between projectile and target dominates the damage effects on the target plate. In order to reproduce the deformation and yield behavior of the structures (RMP and Al plate), the Johnson–Cook strength model, which represents the strength behavior of materials subjected to large strains, high strain rates, and high temperatures, especially in problems of intense impulsive loading due to high-velocity impact, is employed in this study. This model defines the yield stress as

$$\sigma = \left(A + B\varepsilon_p^N\right)\left(1 + C\ln\dot{\varepsilon}_p^*\right)(1 - T_H^m) \tag{13}$$

where ε_p is the effective plastic strain, $\dot{\varepsilon}_p^*$ is the normalized effective plastic strain rate, T_H is the homologous temperature = $(T - T_{room})/(T_{melt} - T_{room})$, and A, B, C, N, and m are five material constants.

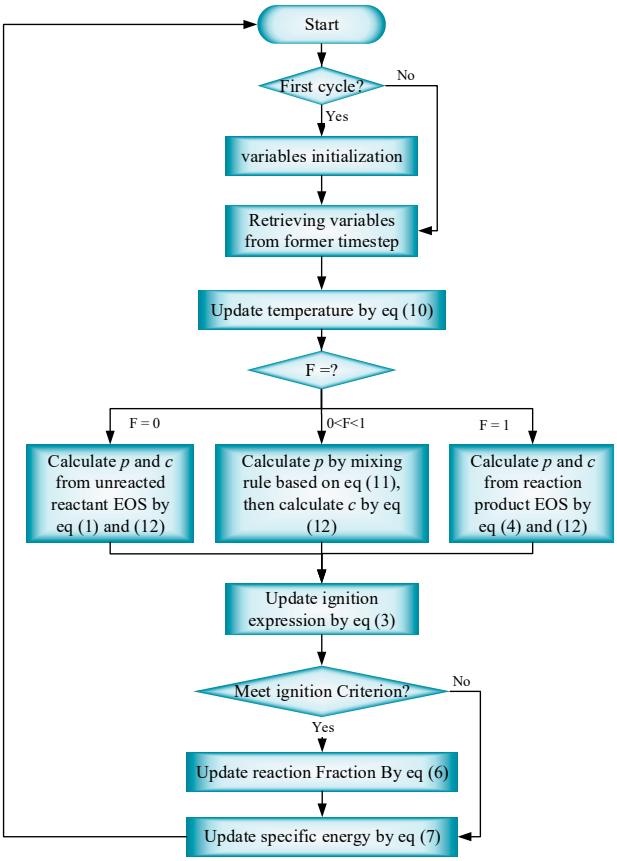

Figure 3. The solve loop of EOS subroutine.

When impacting the target with a high velocity, the projectile may suffer large deformation or even failure as a result of the high pressure caused by this event. The failure of materials means they can resist compressive but not tensile load, so the failure model is often employed to simulate the ejection behavior of fractured debris. Many failure models, such as minimum pressure, principal stress and strain, cumulative damage, and so on, are all permitted in Autodyn code. The Johnson–Cook failure model, which is commonly used to characterize the ductile failure of materials, is employed in this study. It consists of three independent terms that define the dynamic fracture strain as a function of pressure, strain rate, and temperature:

$$\varepsilon^f = \left(D_1 + D_2 e^{D_3 \sigma^*}\right)\left(1 + D_4 \ln \dot{\varepsilon}^*\right)(1 + D_5 T_H), \quad D = \sum \frac{\Delta\varepsilon}{\varepsilon^f} \tag{14}$$

where $\Delta\varepsilon$ is an increment of effective plastic strain, ε_f is failure strain, σ^* is mean stress normalized by the effective stress, and D_1, D_2, D_3, D_4, and D_5 are constants. The Johnson–Cook failure model essentially shows cumulative damage. The ratio of the incremental effective plastic strain to effective fracture strain for a considered particle is defined as the damage factor. The material is assumed to be intact until damage = 1.0. When failure occurs in some particle or element, the contained materials can no longer sustain tension.

3.3. Finite Element Model

The finite element model of RMP impacting double-spaced aluminum plates is shown in Figure 4. The impact and deflagration phenomenon of RMS is a highly nonlinear transient dynamic event; therefore, a meshless SPH method was employed to avoid the interruption

of the simulation, which may be induced by severe deformation or distortion of the meshes used in the Lagrange or Euler methods. The purpose of an SPH method is to describe the continuous material with a group of interacting particles that bear various physical quantities, including mass, speed, etc. By solving the dynamic equation of the group of particles and tracking the movement of each particle track, the mechanical behavior of the whole system can be obtained. In this simulation, the separation distance between particles was set to 0.25 mm, and approximately 11,500 particles were used for the finite element model. The space between the two aluminum plates, one with a thickness of 2 mm and the other 4 mm, was set to 200 mm.

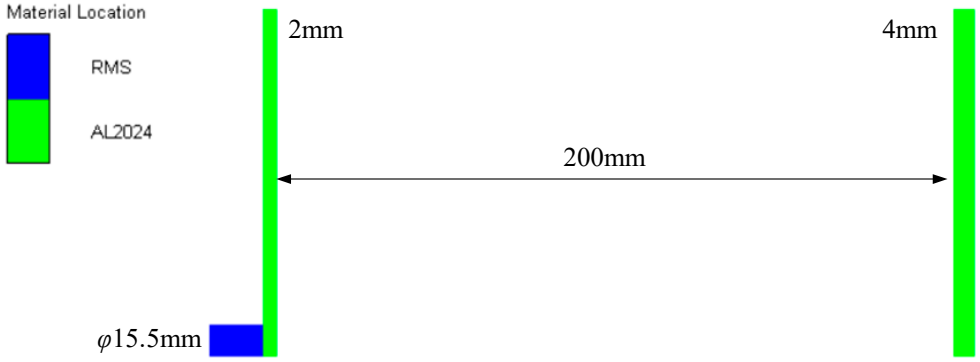

Figure 4. Scheme of simulation model.

4. Result and Discussion

4.1. Penetration Mechanism

The relatively heavier projectile, with a length–diameter ratio of approximately 1:1, produced irregular circular damage patterns on the front side of front plates, which was mainly caused by the unstable flight attitude of RMPs with relatively low kinetic energy. The lighter RMPs, with a length–diameter ratio of approximately 0.5:1, was fabricated to enhance the shot velocity. When the velocity of the RMPs reached above 550 m/s in this study, regular circular penetration holes were found on the front side of the front plates. As analyzed in Refs. [2–26], the RMPs impacting the thin plate with a low velocity were likely to produce petalling damage patterns, whereas high-velocity RMPs impacting thick plates were likely to produce plugging damage patterns. Hence, it is inferred that there is a minimum velocity that intensifies the stress suffered by the plate material to its shear strength, which could lead to the ultimate plugging damage. The relevant mechanisms may be considered as follows.

Generally, if the stress generated in the target plate material in contact with the cylindrical part of the projectile at low velocity is less than the shear strength of the target plate material in the early part of the impact, then the material does not fracture until it moves with the projectile for some distance, resulting in the petalling damage pattern on the plate. A higher velocity increases the stress to the shear strength of the target immediately after impact, resulting in the plugging damage pattern instead. In addition, when the aluminum plate is impacted at a velocity that produces plugging damage, two shockwaves propagate forward into the target and backward into the projectile. Because the considered impact velocity (<600 m/s) is much lower than the propagation velocity of shockwaves (>6000 m/s), the homogeneous stress in the Al plate is formed in a very short time compared to the penetration time, so it is reasonable to assume that every particle velocity in the plugger is the same. Furthermore, the plugger velocity, or the penetration velocity, reaches a steady level shortly after the initial impact time, so one can take the penetration velocity as a constant under the current impact conditions. The force equilibrium relationship on the plugger can be described as

$$\frac{\rho_p C_p \rho_t C_t (v_{0p} - v_{0t})}{\rho_p C_p + \rho_t C_t} A_s = \tau \cdot A_l \tag{15}$$

where ρ and C are density and sound speed of related material, respectively; v_0 is the initial velocity of related material; A_s is the contact area on the impact interface; A_l and τ are the lateral area of the plugger and the shear stress implied on it, respectively; and the subscripts p and t denote the projectile and target, respectively.

The left side of Equation (16) represents the force that accelerates the plugger, whereas the right side is the resistance to the penetration. If the value of the left side is larger than that of the right side, or, for the given materials of projectile and target, if the velocity difference between them is high enough to produce a force exceeding the resistance force produced by the shear strength of the target plate, the plugger is formed immediately after impact; otherwise, the projectile will fly with the target in the vicinity of the impact interface for a longer distance before a penetration hole is formed. In the latter case, more remarkable bulges are found (as shown in Table 1), and petalling damage is produced. Taking τ as the value of the shear strength of the plate material, one can calculate the minimum velocity for plugging damage from Equation (15) for the known projectile and target materials, the diameter of projectile, and the target thickness. The contact area A_s is usually larger than the initial section area of projectile as a result of a mushrooming effect. In this study, we considered A_s the initial section area for simplification, $A_s = \pi D^2/4$, and the lateral area of the plugger was considered $A_l = \pi Dh$. Additionally, it is important to mention that the strain rate effect led to a higher shear strength of the considered materials, so a higher velocity was required for RMPs to produce plugging damage. Substituting the parameters into Equation (15), especially when $v_{0t} = 0$, one can obtain a simplified linear relationship between the minimum velocity for plugging damage and target plate thickness h for given projectile diameter D,

$$v_{0p} = 4\tau' h \frac{\rho_p C_p + \rho_t C_t}{\rho_p C_p \rho_t C_t D} \tag{16}$$

where τ' denotes the dynamic shear strength. Under current experiment conditions, we calculated v_{0p} to equal 496 m/s when taking τ' as 200 Mpa, which is reasonable because the minimum velocity for plugging damage in our experiments was between 401 and 550 m/s.

4.2. The Impact-Induced Deflagration Behavior

A high-speed camera was employed to investigate the impact-induced deflagration event produced by RMPs, the typical pictures are listed in Figures 5 and 6. As shown, a strong fire light is observed immediately after the impact event, indicating that the deflagration reaction is induced by the impact on the front plate. The fire light lasted several hundred microseconds, then gradually fades, and the residual fragments appear in Figures 5 and 6c. The residual fragments impact the rear plate with a relatively low velocity in the following moments, resulting in a more powerful deflagration reaction subsequently. At this time, the fire light lasts for an extended period, several milliseconds, implying more chemical energy was released after the second impact. Finally, the impact-induced deflagration reaction is finished, with the fire light fading away. The deflagration times for the impact on the front and rear plate are shown in Table 1.

The characteristics of fire light, such as appearance time, intensity, size, and so on, are closely related to the ignition and reaction ratio of RMPs. However, because of the shielding effect of fire light and insufficient testing methods at present, it is extremely difficult to study the ignition and relevant reaction mechanisms of RMPs in a high-velocity impact event. Based on this consideration, the numerical simulation method was developed to reproduce the impact-induced deflagration behavior using computer codes. An EOS with tunable ignition threshold was written in Autodyn codes for RMs, and simulations were carried out under the same conditions as the impact experiments, the results of which are shown in Figures 5 and 6. In the pictures, the scale represents the reaction ratio (ALPHA) of every particle included in the simulation model. In this way, the ignition behavior, time-resolved reaction ratio, and temperature distribution of RMPs were obtained. The energy and error time histories are illustrated in Figure 7, which indicates the energy balance at a good level, and the simulation results discussed in detail in the following part is reasonable.

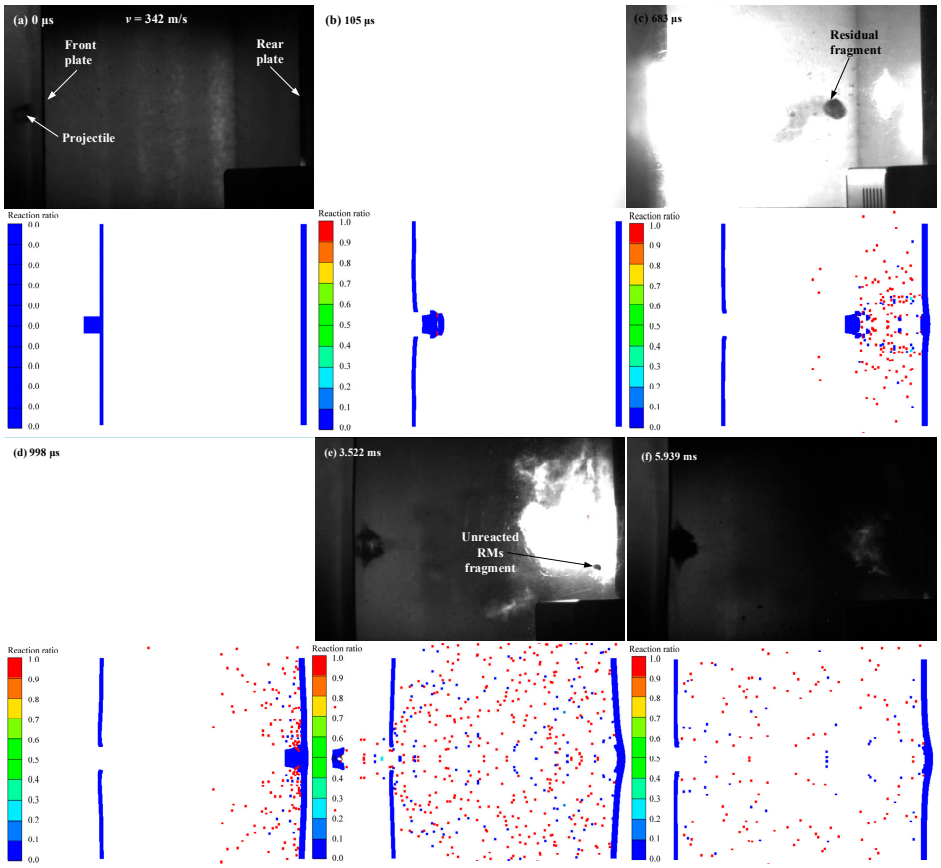

Figure 5. The impact-induced deflagration behavior of RMP with a velocity of 342 m/s.

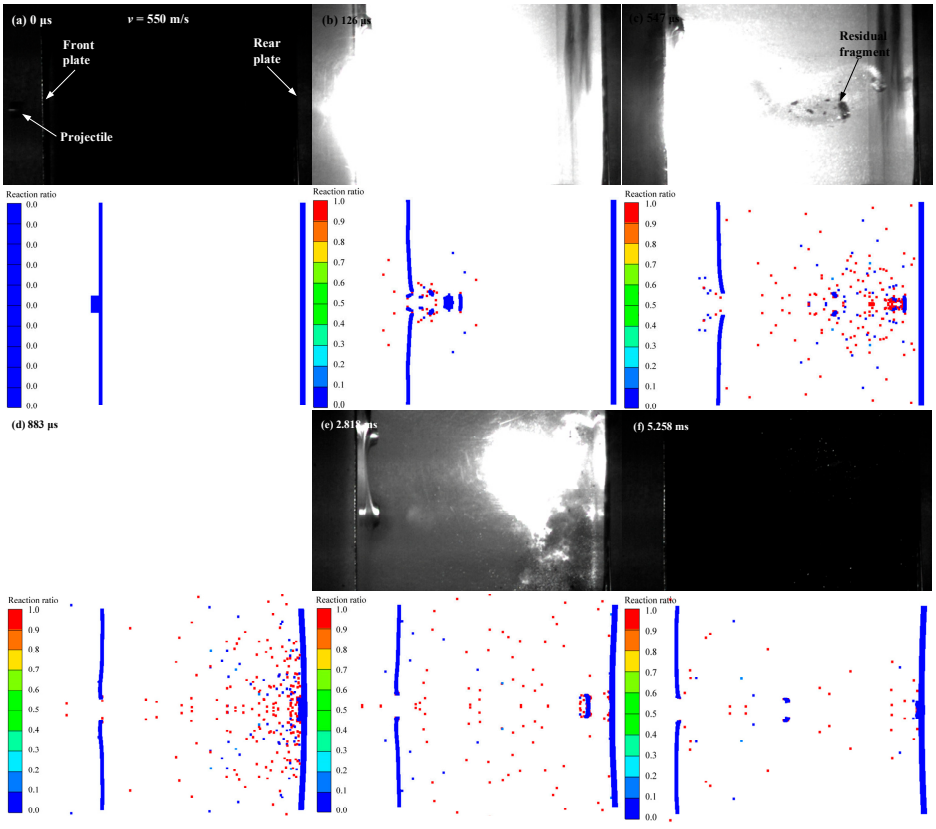

Figure 6. The impact-induced deflagration behavior of RMP with a velocity of 550 m/s.

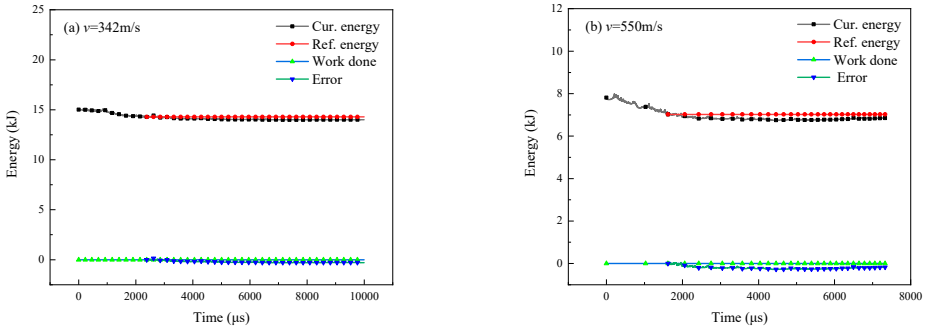

Figure 7. The energy and error versus time histories.

4.3. The Ignition Behavior

Generally, RMs are considered impact-initiated materials, so high-dynamic mechanical load is likely to be required to ignite RMs. In this impact-initiation scenario, one-dimensional impact stress is characterizing the ignition behavior [15,16]. However, quasi-static compression after a specific heat treatment procedure for RMs is also a resultful way to induce the rapid deflagration [26,27], though the chemical reaction may be suspended a short time after ignition because it is difficult to propagate the deflagration in high-density RMs, which may be attributed to the relatively lower deflagration pressure compared to high-energy explosives. Additionally, the ignition behavior of thermal, optical, and electrical stimuli can be found in Refs. [28–33]. In essence, the RMs could be successfully ignited when suffering enough energy stimuli. Based on the above analysis, we determined that the equivalent plastic stress and temperature are the main factors that dominate the ignition behavior of RMPs.

Figures 8 and 9 illustrate the typical ignition process of RMs at 160 μs after impact. When impacting the plate at 342 m/s, the ignition occurs at the strongest shear zone between the edge of the RMP and Al plate immediately after impact (Figure 8b). Then more RMs are activated to deflagration on the fracture surface (Figure 8d). It is interesting to note that the front side of the RMP fails to ignite, though it suffers the maximum pressure during the impact event, resulting in a cone of uninitiated RM fragments flying toward the rear plate. This phenomenon confirms that the ignition mechanisms of RMs are more likely to be attributed to shear instead of pressure, because the ignition result in this simulation is well consistent with the experiment result by Raftenberg [34]. When the impact velocity is enhanced to 550 m/s, more RMs are activated as a result of stronger shear effects between the edge of the RMP and plate (Figure 9d). Nevertheless, several RM fragments still fail to ignite (Figure 9e).

The relevant ignition mechanism can be analyzed based on the curves of ignition indicator, reaction ratio, pressure, and temperature versus time at the gauges set on the front side of the RMPs, as shown in Figures 8f and 9f. A high-pressure pulse is produced first after impact. However, we use equivalent plastic stress as the indicator of ignition. The equivalent plastic stress is divided into two parts in Autodyn. One part is hydrostatic pressure calculated by EOS; the other is deviator stress calculated by a constitutive model. Although the pressure is high, the integral indicator of ignition constant does not increase remarkably, indicating that the required stress threshold has not been reached at this time. After this, the forward-propagating compression wave is reflected by the free surface of the front plate, resulting in a rarefaction wave propagating backward to the RMP, which leads to a sharp decline in pressure on the materials. The rarefaction wave may also enhance the particle velocity change in the RMP, which causes high stress in RMs. Then, the indicator of ignition increases linearly to the value set by user (the value was set to one in this study). At this time the deflagration is successfully induced, and the pressure of the mixture of reactant and deflagration product is calculated based on the pressure and temperature equilibrium. As a result of the deflagration, massive chemical energy is released. The released energy exists in the form of pressure, potential energy, and internal energy. The pressure and

temperature are remarkably enhanced by the increase of reaction ratio ALPHA. As shown in Figures 8f and 9f, when ALPHA increases to one, which indicates the deflagration stops at this time, the pressure and temperature of the particle present a declining trend.

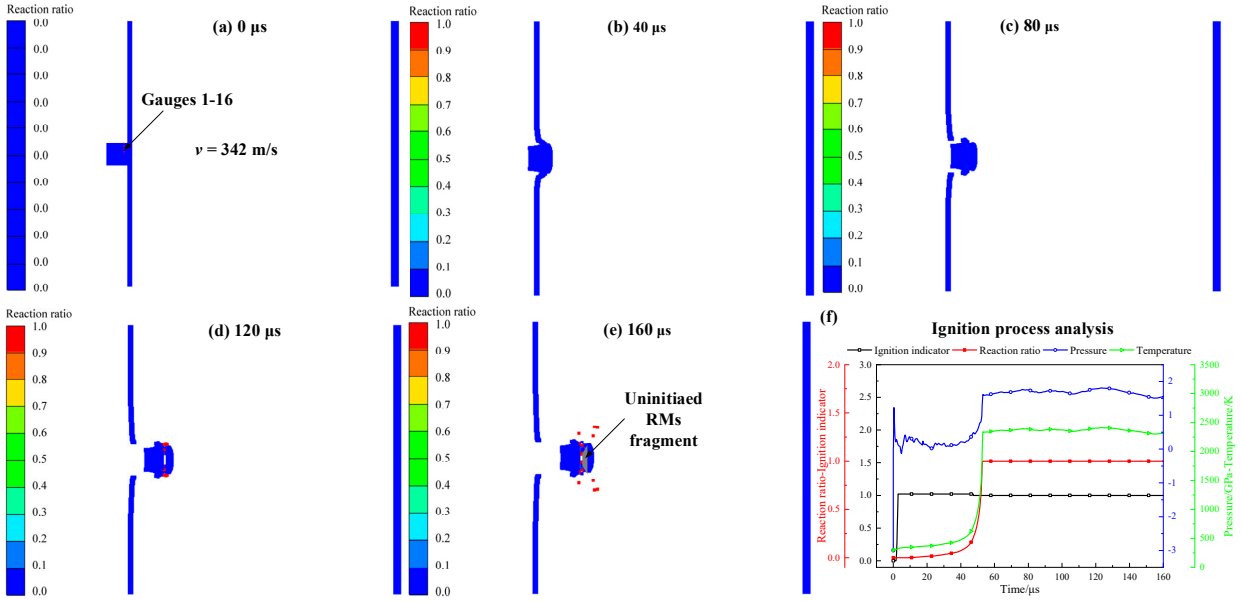

Figure 8. The ignition process of RMPs with a velocity of 342 m/s.

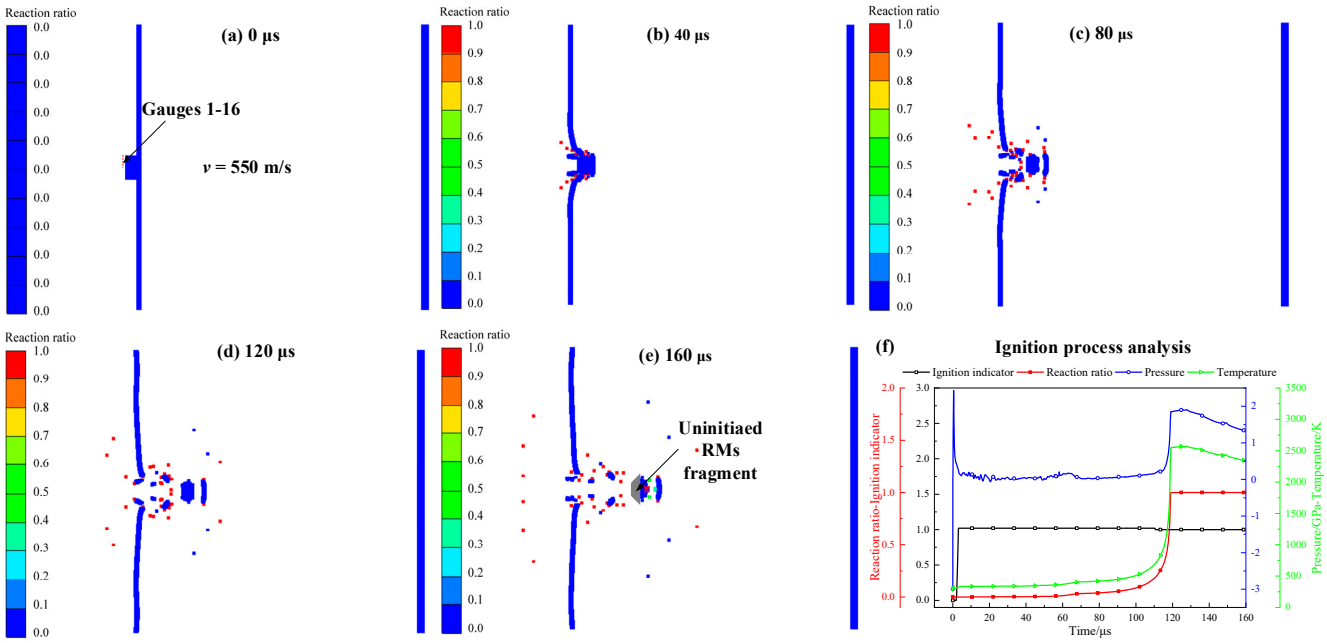

Figure 9. The typical ignition process of RMPs with a velocity of 550 m/s.

4.4. The Energy Release Behavior of RMPs

The energy release behavior of RMPs can be represented by a time-resolved reaction ratio. To get a time-resolved reaction ratio of an RMP for quantity research in the penetration and deflagration process, a subroutine executed at the end of every calculation circulation is compiled. The reaction ratio of an RMP is defined as

$$F = \frac{\sum m_i \alpha_i}{\sum m_i} \tag{17}$$

where m_i denotes the mass of every particle contained in the RMP and α_i corresponds to the reaction ratio of the particles.

The time-resolved reaction ratio of an RMP with an impact velocity of 342 and 550 m/s is shown in Figure 10. As analyzed above, the deflagration starts when the indicator of ignition constant reaches the preset value. After perforating the front plate, the reaction ratio of RMPs increases remarkably. Then, however, there is an approximate flat in the curve of the reaction ratio of RMPs, which implies the flameout of overall deflagration. This simulation result can be verified by the sharp decay of fire light in the experiments, and it does not greatly change until the residual RM fragments impact the rear plate. Then, partial RMs ignite at the second impact and the reaction ratio increases to a new level. It can be also seen from the pictures that the deflagration quantity after impact on the front and rear plate is dependent on impact velocity. When the impact velocity is 340 m/s, the deflagration quantity after impact on the front plate is less than 550 m/s (the reaction ratio rises to 9% for 340 m/s while 19% for 550 m/s). The indicator of ignition constants of uninitiated RMs accumulated during the first impact, so the impact on the rear plate induces more RMs to be deflagrated. The final reaction ratio increases with the impact velocity, but neither their final reaction ratio nor reaction efficiency reaches one, indicating that partial RMs in the RMP fail to ignite under current impact conditions.

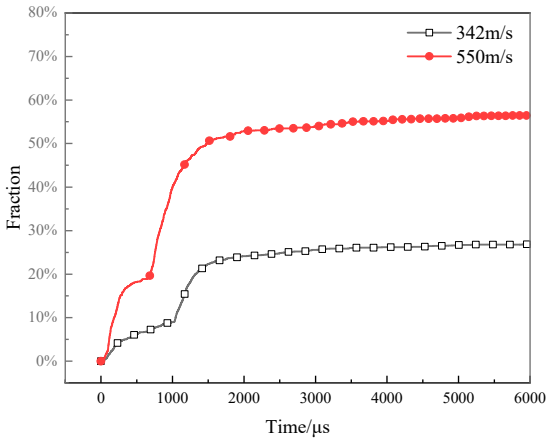

Figure 10. The time-resolved reaction ratio of RMP versus time.

The fragmentation of the RMs projectile is likely the prerequisite condition for ignition because of the non-self-sustaining reaction in RMs. The fragmentation is mainly caused by accumulation of damage related to the plastic deformation or plastic work. From Figure 10, one can conclude that the higher deflagration reaction degree includes two parts. First, after perforating the first plate, the plastic work absorbed by the cylindrical surface of the projectile is higher, inducing more RMs to react. Second, on the front of the rear plate, more reaction is induced. The reason may be that more damage has been produced inside the projectile after perforating the first plate with a higher velocity, and the higher residual velocity of RMs will also produce more serious fragmentation of RMs inside the residual penetration body after impact on the rear plate, resulting in higher reaction degree of the RMs projectile.

4.5. The Temperature Rise Effect

According to the first law of thermodynamics, the massive chemical energy released by the deflagration reaction will be transformed into pressure, potential energy, and internal energy of deflagration product. High pressure can cause the rapid expansion of product while internal energy heats the product to a high temperature. The early evolution of pressure and temperature is shown in Figures 8f and 9f. In Figure 11, the later temperature distribution of RMs at the impact on the rear Al plate is shown. The maximum steady temperatures are 2901 and 3154 K for the impact velocities 342 and 550 m/s, respectively.

This temperature is consistent with the results captured by the infrared framing camera and transient pyrometer in Ref. [8]. The chemical energy released during the impact process can be estimated as

$$4Al + 3(-C_2F_4-) \rightarrow 4AlF_3 + 6C + 2379.61\ kJ \quad (18)$$

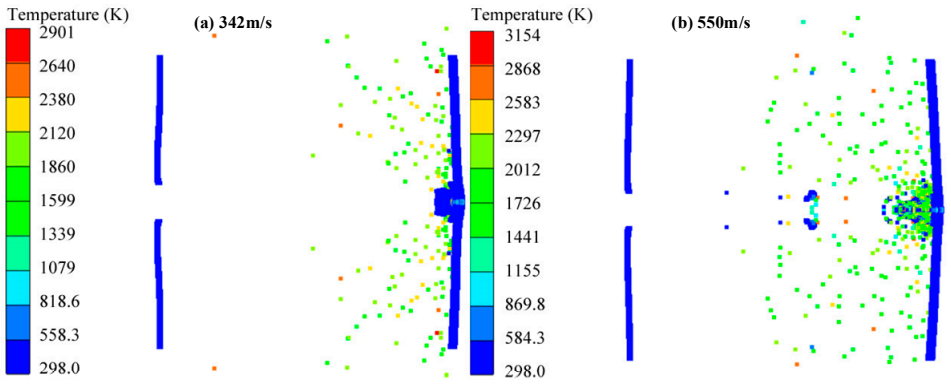

Figure 11. The temperature distribution at impact on the rear plate.

Assuming that the released chemical energy is absolutely transferred to internal energy of deflagration products, then the temperature could be estimated considering specific heat capacity of the deflagration products. Taking the values of the specific heat capacities of AlF_3 and C as 100.831 and 21.609 J/mol·K, respectively, the calculated temperature for the deflagration products is approximately 4464 K. The lower temperature in the simulation can be attributed to persistent expansion of the particles during or after impact, which leads to external work acting on surrounding particles, resulting in a cooling effect for relevant particles according to the first law of thermodynamics.

5. Conclusions

To understand the mechanisms of impact-induced deflagration reactions by RMPs more clearly, a simulation method is presented in this study. High-velocity impact experiments were performed to prove the validity of the simulations. The ignition indicator, reaction ratio, pressure, and temperature distribution are analyzed in detail. The results show that the equivalent plastic stress is more likely to dominate the ignition of RMs instead of the high-pressure pulse produced immediately after impact, because no remarkable increase of the ignition indicator was observed when the pressure reached its maximum value during impact. The history curve of reaction ratio and temperature distribution of RMPs was obtained using a numerical simulation. The increasing trend of the reaction ratio is well consistent with the change of radiated fire light in experiments, and the calculated temperature is reasonable compared to experiment results reported in other studies. In summation, the presented simulation method is able to reproduce the impact-induced deflagration behavior of a reactive materials projectile.

Author Contributions: Conceptualization, J.X. and X.L., methodology, C.H.; software, J.X.; formal analysis, D.Z.; data curation, Y.W.; writing—original draft preparation, J.X.; writing—review and editing, X.L.; funding acquisition, J.X. All authors have read and agreed to the published version of the manuscript.

Funding: The research was funded by National Natural Science Foundation of China (Grant No. 11702256), Natural Science Foundation of Shanxi Province (Grant No. 20210302124214), Scientific and Technological Innovation Programs of Higher Education Institutions in Shanxi (Grant No. 201802071), and Scientific and Technological Innovation Team Programs of North University of China (Grant No.TD201903).

Institutional Review Board Statement: Not applicable.

Informed Consent Statement: Not applicable.

Data Availability Statement: The data that support the findings of this study are available from the corresponding author upon reasonable request.

Conflicts of Interest: The authors declare no conflict of interest.

References

1. Ames, R.G. Vented chamber calorimetry for impact-initiated energetic materials. *43rd AIAA Aerosp. Sci. Meet. Exhib.-Meet. Pap.* **2005**, 15391–15403. [CrossRef]
2. Zheng, Y.; Zheng, Z.; Lu, G.; Wang, H.; Guo, H. Mesoscale study on explosion-induced formation and thermochemical response of PTFE/Al granular jet. *Def. Technol.* **2022**. [CrossRef]
3. Rosencrantz, S.D. Characterization and Modeling Methodology of Polytetrafluoroethylene Based Reactive Materials for the Development of Parametric Models. Ph.D. Thesis, Wright State University, Dayton, OH, USA, 2007.
4. Guo, H.; Zheng, Y.; Yu, Q.; Ge, C.; Wang, H. Penetration behavior of reactive liner shaped charge jet impacting thick steel plates. *Int. J. Impact Eng.* **2019**, *126*, 76–84. [CrossRef]
5. Liu, S.B.; Yuan, Y.; Zheng, Y.F.; Ge, C.; Wang, H.F. Enhanced ignition behavior of reactive material projectiles impacting fuel-filled tank. *Def. Technol.* **2019**, *15*, 533–540. [CrossRef]
6. Zheng, Y.; Su, C.; Guo, H.; Yu, Q.; Wang, H. Behind-Target Rupturing Effects of Sandwich-like Plates by Reactive Liner Shaped Charge Jet. *Propellants Explos. Pyrotech.* **2019**, *44*, 1400–1409. [CrossRef]
7. Xiao, J.; Zhang, X.; Guo, Z.; Wang, H. Enhanced Damage Effects of Multi-Layered Concrete Target Produced by Reactive Materials Liner. *Propellants Explos. Pyrotech.* **2018**, *43*, 955–961. [CrossRef]
8. Xiao, J.; Nie, Z.; Wang, Z.; Du, Y.; Tang, E. Energy release behavior of Al/PTFE reactive materials powder in a closed chamber. *J. Appl. Phys.* **2020**, *127*, 165106. [CrossRef]
9. Canonsburg, T.D. Application of CFD into an automotive torque converter. *Knowl. Creat. Diffus. Util.* **2012**, *15317*, 724–746.
10. Wang, H.F.; Zheng, Y.F.; Yu, Q.B.; Liu, Z.W.; Yu, W.M. Study on initiation mechanism of reactive fragment to covered explosive. *Beijing Ligong Daxue Xuebao/Trans. Beijing Inst. Technol.* **2012**, *32*, 786–823.
11. Raftenberg, M.N.; Mock, W.; Kirby, G.C. Modeling the impact deformation of rods of a pressed PTFE/Al composite mixture. *Int. J. Impact Eng.* **2008**, *35*, 1735–1744. [CrossRef]
12. Yang, S.-Q.; Xu, S.-L.; Zhang, T. Preparation and Performance of PTEF/Al Reactive Materials. *J. Natl. Univ. Def. Technol.* **2008**, *30*, 39–42.
13. Jiang, J.-W.; Wang, S.-Y.; Zhang, M.; Wei, Q. Modeling and simulation of JWL equation of state for reactive Al/PTFE mixture. *J. Beijing Inst. Technol.* **2012**, *21*, 150–156.
14. Lee, E.L.; Tarver, C.M. Phenomenological model of shock initiation in heterogeneous explosives. *Phys. Fluids* **1980**, *23*, 2362–2372. [CrossRef]
15. Mock, W.; Holt, W.H. Impact initiation of rods of pressed polytetrafluoroethylene (PTFE) and aluminum powders. *AIP Conf. Proc.* **2006**, *845*, 1097–1100.
16. Mock, W.; Drotar, J.T. Effect of aluminum particle size on the impact initiation of pressed PTFE/Al composite rods. *AIP Conf. Proc.* **2007**, *955*, 971–974.
17. Zhang, X.P.; Xiao, J.G.; Yu, Q.B.; Zheng, Y.F.; Wang, H.F. Demolition effect of reactive material liner shaped charge against concrete target. *Beijing Ligong Daxue Xuebao/Trans. Beijing Inst. Technol.* **2016**, *36*, 1211–1215.
18. Yi, J.; Wang, Z.; Yin, J.; Zhang, Z. Simulation study on expansive jet formation characteristics of polymer liner. *Materials* **2019**, *12*, 744. [CrossRef]
19. Zhang, X.F.; Shi, A.S.; Qiao, L.; Zhang, J.; Zhang, Y.G.; Guan, Z.W. Experimental study on impact-initiated characters of multifunctional energetic structural materials. *J. Appl. Phys.* **2013**, *113*, 083508. [CrossRef]
20. Su, C.; Wang, H.; Xie, J.; Ge, C.; Zheng, Y. Penetration and Damage Effects of Reactive Material Jet against Concrete Target. *Binggong Xuebao/Acta Armamentarii* **2019**, *40*, 1829–1835.
21. Zhang, Z.Y.; Tian, Z.D.; Chen, J.; Duan, Z.P. *Detonation Physics*; National University of Defense Technology Press: Changsha, China, 2016; p. 270.
22. Lee, E.L.; Hornig, H.C.; Kury, J.W. *Adiabatic Expansion of High Explosive Detonation Products*; Report UCRL-50422; Lawrence Radiation Labroratory of University of California: Livermore, CA, USA, 1968.
23. Xu, F.Y.; Zheng, Y.F.; Yu, Q.B.; Wang, Y.Z.; Wang, H.F. Experimental study on penetration behavior of reactive material projectile impacting aluminum plate. *Int. J. Impact Eng.* **2016**, *95*, 125–132. [CrossRef]
24. Xu, F.Y.; Zheng, Y.F.; Yu, Q.B.; Zhang, X.P.; Wang, H.F. Damage effects of aluminum plate by reactive material projectile impact. *Int. J. Impact Eng.* **2017**, *104*, 38–44. [CrossRef]
25. Xu, F.Y.; Yu, Q.B.; Zheng, Y.F.; Lei, M.A.; Wang, H.F. Damage effects of double-spaced aluminum plates by reactive material projectile impact. *Int. J. Impact Eng.* **2017**, *104*, 13–20. [CrossRef]
26. Feng, B.; Li, Y.; Wu, S.; Wang, H.; Tao, Z.; Fang, X. A crack-induced initiation mechanism of Al-PTFE under quasi-static compression and the investigation of influencing factors. *Mater. Des.* **2016**, *108*, 411–417. [CrossRef]

27. Feng, B.; Fang, X.; Li, Y.C.; Wang, H.X.; Mao, Y.M.; Wu, S.Z. An initiation phenomenon of Al-PTFE under quasi-static compression. *Chem. Phys. Lett.* **2015**, *637*, 38–41. [CrossRef]
28. Sippel, T.R.; Son, S.F.; Groven, L.J. Aluminum agglomeration reduction in a composite propellant using tailored Al/PTFE particles. *Combust. Flame* **2014**, *161*, 311–321. [CrossRef]
29. Osborne, D.T.; Pantoya, M.L. Effect of Al particle size on the thermal degradation of Al/Teflon mixtures. *Combust. Sci. Technol.* **2007**, *179*, 1467–1480. [CrossRef]
30. Mohan, S.; Trunov, M.A.; Dreizin, E.L. Heating and ignition of metallic particles by a CO_2 laser. *J. Propuls. Power* **2008**, *24*, 199–205. [CrossRef]
31. Wu, Y. *Study on Reaction Heat Measuring and Energy Release Characteristics of PTFE/Al Reactive Material*; National University of Defense Technology: Changsha, China, 2015.
32. Dolgoborodov, A.Y.; Makhov, M.N.; Kolbanev, I.V.; Streletskiĭ, A.N.; Fortov, V.E. Detonation in an aluminum-teflon mixture. *JETP Lett.* **2005**, *81*, 311–314. [CrossRef]
33. Dolgoborodov, A.Y.; Makhov, M.N.; Streletskii, A.N.; Kolbanev, I.V.; Gogulya, M.F.; Brazhnikov, M.A.; Fortov, V.E. Detonation-like phenomena in non-explosive oxidizer-metal mixtures. In Proceedings of the 31st International Pyrotechnics Seminar, Fort Collins, CO, USA, 11–16 July 2004; p. 569.
34. Raftenberg, M.N.; Scheidler, M.J.; Casem, D.A. *A Yield Strength Model and Thoughts on an Ignition Criterion for a Reactive PTFE-Aluminum Composite*; Report ARL-RP-219; Army Research Laboratory: Aberdeen Proving Ground, MD, USA, 2008.